

A Class of Inertial Measurement Units for Low-Noise Angular Velocity Estimation

Konstantinos Papafotis¹, Member, IEEE, Dimitris Nikitas², Graduate Student Member, IEEE, Costas Oustoglou¹, and Paul P. Sotiriadis², Fellow, IEEE

Abstract—An inertial measurement unit (IMU) architecture estimating angular velocity is introduced. It expands the concept of multiaccelerometers gyroscope-free IMUs (GF-IMUs), taking the advantage of their excellent noise performance and resolving their inability to compensate for accelerometers' bias and their requirement for specific accelerometers placement, which makes GF-IMUs inappropriate for real-world applications. It does so by embedding the accelerometers in a low-bandwidth closed-loop configuration with a three-axis gyroscope and by addressing the complete nonlinear dynamics. An extensive theoretical analysis provides a complete framework for designing low-noise IMUs, including sufficient stability criteria for the nonlinear system's dynamics. Simulation and experimental results support the theoretical analysis and indicate that even a minimal system using the proposed architecture can outperform the gyroscope in noise performance by at most 15 dB in some frequency range.

Index Terms—Accelerometer, gyroscope, inertial measurement unit (IMU), low noise.

I. INTRODUCTION

THE rapid advancement of the microelectromechanical (MEM) accelerometers and gyroscopes over the past decades made inertial sensors a key part of several electronic devices. Nowadays, MEM inertial sensors are used in a wide range of applications, from commercial devices to high-end, industrial and military ones. Despite their size and cost characteristics, which make MEM inertial sensors suitable for many applications, their big measurement error [1] must be compensated when accuracy is required.

A big part of the measurement error of an inertial sensor is static and caused by imperfections of the mechanical and electronic structures of the sensor. The static error is

Manuscript received 5 December 2022; accepted 14 January 2023. Date of publication 13 February 2023; date of current version 3 March 2023. This work was supported in part by Greece and the European Union (European Social Fund—ESF) through the Operational Program “Human Resources Development, Education and Lifelong Learning” within the Project “Strengthening Human Resources Research Potential via Doctorate Research,” implemented by the State Scholarships Foundation (IKY), under Grant MIS-5000432; and in part by the European Union-NextGenerationEU and Greek National Funds through the Greece 2.0 National Recovery and Resilience Plan, within the call Research—Create—Innovate, under Project TAEDK-06165. The work of Dimitris Nikitas was supported by the Onassis Foundation under Scholarship FZS 041-1/2022-2023. The Associate Editor coordinating the review process was Dr. Guanfeng Du. (Corresponding author: Konstantinos Papafotis.)

Konstantinos Papafotis, Costas Oustoglou, and Paul P. Sotiriadis are with the Department of Electrical and Computer Engineering, National Technical University of Athens, 15780 Athens, Greece (e-mail: k.papafotis@gmail.com).

Dimitris Nikitas is with the Department of Electrical Engineering, Eindhoven University of Technology, 5600 MB Eindhoven, The Netherlands. Digital Object Identifier 10.1109/TIM.2023.3244216

most commonly modeled as a linear combination of different error terms (bias, nonorthogonality, cross-axis sensitivity, and so on) and can be compensated by using the proper calibration techniques [2], [3], [4], [5], [6], [7], [8], [9]. In addition, a high-performance sensor is commonly calibrated for the dynamic nonlinear temperature dependence of its measurement [10], [11].

On the other hand, compensating for the dynamic measurement errors, such as bias drift and nondeterministic noise, is a more difficult task. To this end, most authors use extra sensors or filtering and estimation techniques to reduce the effect of these errors. As an example, in inertial navigation, it is common to use a magnetometer [12], [13] along with a Kalman filter [1], [14] to compensate for the cumulative attitude error introduced by the gyroscope's measurement errors [15].

Gyroscope-free inertial measurements units (GF-IMUs) estimate the angular velocity of a rigid body using the measurements of multiple accelerometers. A great advantage of GF-IMUs is that as the distance between the accelerometers increases, the noise of the angular velocity estimation becomes lower. Thus, placing the accelerometers in a sufficient distance (see Section IV), a GF-IMU can outperform a gyroscope of the same grade¹ in terms of noise performance.

However, as shown in Section II-B, GF-IMUs have a big disadvantage; they cannot compensate for the accelerometers' bias. More specifically, their open-loop structure translates even a small bias into a cumulative angular velocity error. This is an important restriction for real-world applications, especially when low-cost sensors are considered where the bias drifts significantly over time.

In our previous works [17], [18], we demonstrated how using certain GF-IMU architectures and introducing a three-axis gyroscope in a feedback loop, we overcome the bias drifting problem of GF-IMUs, while we still take advantage of their low-noise characteristics. However, the analysis in [17] and [18] is limited to the cases of specific GF-IMU architectures, such as [19] and [20], where the angular velocity is obtained as the solution of a linear system of differential equations.

In this work, we expand the analysis of [17] and [18] and consider the general case where several accelerometers are

¹Inertial sensors are grouped into four categories (grades) based on their performance characteristics: navigation grade, tactical grade, industrial grade, and automotive grade [16].

placed on a rigid body in arbitrary positions, and the angular velocity is derived as the solution of a nonlinear system of differential equations. Similar to [17] and [18], a three-axis gyroscope is used in a feedback loop to dynamically compensate for the accelerometers' bias. The stability of the proposed closed-loop system is examined analytically, and closed-form conditions are provided. Finally, extensive simulations and experimental measurements reveal the superior noise performance of the proposed system; its angular velocity noise in a 100-Hz bandwidth is about 15 dB lower compared with the one of the gyroscopes making the proposed architecture ideal for applications where higher bandwidth is needed.

The rest of this work is structured as follows. In Section II, the operation principles of GF-IMUs are briefly introduced, and their performance limitations are highlighted. In Section III, the proposed closed-loop, nonlinear architecture is introduced. A detailed theoretical analysis is presented, and stability conditions are provided. In Section IV, the system's performance is tested, and some important design considerations are expressed. Finally, the conclusions are drawn in Section V.

II. GYROSCOPE-FREE IMUS

This section introduces the basic operation principles of GF-IMUs and highlights their performance limitations.

A. Principle of Operation for GF-IMUs

Consider N single-axis accelerometers, placed at arbitrary positions on a rigid body, denoted by r_i , $i = 1, 2, \dots, N$. Their input axes and measurements are denoted as $\hat{\eta}_i \in \mathbb{R}^3$ and $f_i \in \mathbb{R}$, respectively. With respect to the well-used formulation of [20], the specific force ($f \in \mathbb{R}^3$) and the angular velocity ($\omega \in \mathbb{R}^3$) are given as follows:

$$F = Jx + P \quad (1)$$

where

$$x = \begin{bmatrix} \dot{\omega} \\ f \end{bmatrix}, \quad J = \begin{bmatrix} J_1^\top & J_2^\top \end{bmatrix}$$

$$F = \begin{bmatrix} f_1 \\ f_2 \\ \vdots \\ f_N \end{bmatrix}, \quad P = \begin{bmatrix} \hat{\eta}_1^\top \Omega^2 r_1 \\ \hat{\eta}_2^\top \Omega^2 r_2 \\ \vdots \\ \hat{\eta}_N^\top \Omega^2 r_N \end{bmatrix} \quad (2)$$

with the auxiliary variables J_1 and J_2

$$J_1 = \begin{bmatrix} (r_1 \times \hat{\eta}_1) & (r_2 \times \hat{\eta}_2) & \dots & (r_N \times \hat{\eta}_N) \end{bmatrix}$$

$$J_2 = \begin{bmatrix} \hat{\eta}_1 & \hat{\eta}_2 & \dots & \hat{\eta}_N \end{bmatrix} \quad (3)$$

and Ω is the cross-product matrix of the vector $\omega \triangleq [\omega_x \ \omega_y \ \omega_z]^\top$

$$\Omega = \begin{bmatrix} 0 & -\omega_z & \omega_y \\ \omega_z & 0 & -\omega_x \\ -\omega_y & \omega_x & 0 \end{bmatrix}. \quad (4)$$

Using measurements from a sufficient number of properly placed accelerometers, one can solve (1) with respect to x in a least-squares sense as follows:

$$x = (J^\top J)^{-1} J^\top (F - P). \quad (5)$$

For notation ease, we define $\bar{J} = (J^\top J)^{-1} J^\top$, and then, (5) can be written compactly as follows:

$$x = \bar{J}F - \bar{J}P \quad (6)$$

in which the solution is only meaningful for nonsingular $J^\top J$.

For GF-IMUs, the interest is to derive the angular velocity, ω . Denoting the i th row of \bar{J} as \bar{J}_i , we write

$$\dot{\omega} = \hat{J}F - \hat{J}P \quad (7)$$

in which

$$\hat{J} = \begin{bmatrix} \bar{J}_1^\top & \bar{J}_2^\top & \bar{J}_3^\top \end{bmatrix}^\top. \quad (8)$$

B. Existing Art and Performance Limitations

Over the years, different architectures using six [20], nine [19], [21], [22], ten [23], or 12 [24], [25] (single-axis) accelerometers have been proposed, reaching to a feasible solution for (7). However, in the existing works, only very specific geometries for the accelerometers' placement were considered in an effort simplifying the original nonlinear angular velocity estimation problem (7) to a linear one. In those specific configurations, the nonlinear terms of (7) are eliminated (i.e., $\hat{J}P = \bar{0}$), and thus, the angular velocity is estimated by $\dot{\omega}_i = \hat{J}F$. As demonstrated in [17] and [18], the presence of arbitrarily small static bias in accelerometers' measurements (1) yields a cumulative estimation error, which eventually diverges. Note that, this applies even for calibrated instruments, since a small bias drift is expected over time.

III. PROPOSED SYSTEM

This section introduces the proposed inertial measurement architecture and provides the detailed dynamics analysis. Easy-to-check conditions to ensure the stability of the proposed system under the effects of the gyroscopes' and accelerometers' biases are provided.

A. System Architecture

To mitigate the arising issues of existing architectures, as underlined in Section II-B, the proposed architecture combines multiple single-axis accelerometers with a single three-axis gyroscope in a closed-loop configuration. The top-level architecture of the proposed system is shown in Fig. 1.

In Fig. 1, we consider the general case of an arbitrary configuration of $N > 6$ single-axis accelerometers, and thus, the nonlinear feedback term $\hat{J}P$ of (6) is also included. A second feedback loop compares the angular velocity calculated using the accelerometers' measurements and the GF-IMU theory with the measurement of the gyroscope and forces the lower-frequency part of the system's estimation (ω) to follow the gyroscope's measurement. In higher frequencies, the error-based feedback signal coming from the upper loop structure is attenuated, and the system outputs the angular velocity estimated using the accelerometers' measurements. By doing so, the proposed system ensures that the constant accelerometers' bias does not affect the system's output, whereas in the higher-frequency range, the system outputs

$$\Delta = \begin{bmatrix} \delta_1 \\ \delta_2 \\ \vdots \\ \delta_N \end{bmatrix}, \quad E = \begin{bmatrix} \epsilon_1 \\ \epsilon_2 \\ \vdots \\ \epsilon_N \end{bmatrix}, \quad Z = \begin{bmatrix} \zeta_1 \\ \zeta_2 \\ \vdots \\ \zeta_N \end{bmatrix}. \quad (16)$$

Now, considering the proposed system of Fig. 1 and replacing (15) into (7), we write

$$\dot{\omega} = \hat{J}F - ML(\omega) - G\omega_f \quad (17)$$

where the filter's dynamics, similar to (11), are described by

$$\dot{\omega}_f = -P_p \omega_f + P_p(\delta\omega - \delta\omega_g) \quad (18)$$

and the ground truth angular velocity is given by

$$\dot{\omega}_{gi} = \hat{J}F - ML(\omega_{gi}). \quad (19)$$

We formulate the output error's dynamics as in the linear case. Considering $\delta\omega = \omega - \omega_{gi}$, we have

$$\dot{\delta\omega} = -M(L(\omega) - L(\omega_{gi})) + \hat{J}\delta F - G\omega_f. \quad (20)$$

By substituting $\omega = \delta\omega + \omega_{gi}$, we get

$$\begin{aligned} L(\omega) - L(\omega_{gi}) &= K(\omega_{gi})\delta\omega + L(\delta\omega) \\ &= K(\omega_{gi})\delta\omega + O(\|\delta\omega\|^2) \end{aligned} \quad (21)$$

where

$$K(\omega_{gi}) = \begin{bmatrix} -2\omega_{gi}^x & 0 & 0 \\ 0 & -2\omega_{gi}^y & 0 \\ 0 & 0 & 2\omega_{gi}^x \\ \omega_{gi}^y & \omega_{gi}^x & 0 \\ \omega_{gi}^z & 0 & \omega_{gi}^x \\ 0 & \omega_{gi}^z & \omega_{gi}^y \end{bmatrix}. \quad (22)$$

Neglecting the higher order terms in (21), we rewrite (20) as follows:

$$\dot{\delta\omega} = -MK(\omega_{gi})\delta\omega + \hat{J}\delta F - G\omega_f. \quad (23)$$

Using (23) and (18), we write the following state-space representation for the proposed system:

$$\underbrace{\begin{bmatrix} \dot{\delta\omega} \\ \dot{\omega}_f \end{bmatrix}}_x = \underbrace{\begin{bmatrix} -MK(\omega_{gi}) & -G \\ P_p & -P_p \end{bmatrix}}_A \underbrace{\begin{bmatrix} \delta\omega \\ \omega_f \end{bmatrix}}_x + \underbrace{\begin{bmatrix} \hat{J} & 0_{3 \times 3} \\ 0_{3 \times 6} & -P_p \end{bmatrix}}_B \underbrace{\begin{bmatrix} \delta F \\ \delta\omega_g \end{bmatrix}}_u. \quad (24)$$

Comparing (24) with (11), we notice that the only difference is the North–West block in matrix A . This block depends on the actual angular velocity vector ω_{gi} and is of course time-varying. As a result, we have to further investigate the stability of the autonomous part of the system (i.e., $\dot{x} = Ax$), which is strongly related to BIBO stability [27], [28]. To this end, and since the system of (24) can be seen as quasi-linear [29], [30], we touch upon on some well-established results in linear parameter-varying (LPV) system's theory [31], [32], [33].

To start with, we define the time-varying parameters $\delta_i \triangleq \omega_{gi}^i$ for $i = 1, 2, 3$ and so as A is a parameter-varying matrix (i.e., $A \triangleq A(\delta_1, \delta_2, \delta_3)$). These parameters appear in an affine way in A , i.e.,

$$A = A_0 + A_1\delta_1 + A_2\delta_2 + A_3\delta_3. \quad (25)$$

Considering that the angular velocity of the object is bounded, the parameters δ_i , $i = 1, 2, 3$ are also considered to be bounded, i.e., $|\delta_i| \leq \delta_{\max}$. Hence, the parameter vector $\delta = [\delta_1 \ \delta_2 \ \delta_3]^\top \in \mathcal{D} = \text{co}(\delta^1, \delta^2, \dots, \delta^8)$, with $\delta^j \in \mathbb{R}^3$ for $j = 1, 2, \dots, 8$, where $\text{co}(\cdot)$ denotes the convex hull of vertices δ^j [34]. In our case, \mathcal{D} composes a cube centered at zero with vertices $\{\pm\delta_{\max}, \pm\delta_{\max}, \pm\delta_{\max}\}$. Furthermore, we define the set of vertices $\mathcal{D}_l = \{\delta^1, \delta^2, \dots, \delta^8\}$.

The parametric-varying system $\dot{x} = A(\delta)x$ with $\delta \in \mathcal{D}$ is exponentially stable if [31] $\exists X \in \mathbb{R}^{6 \times 6}, X > 0^2$

$$A^\top(\delta)X + XA(\delta) < 0 \quad \forall \delta \in \mathcal{D}. \quad (26)$$

Using (26), one can in theory prove the stability of the proposed system by solving an infinite number of linear matrix inequalities (LMIs). In our case, however, the stability conditions can be relaxed, and use only a finite amount of LMIs [31], [33]. Considering that $A(\delta)$ is affine on parameter vector δ , the parametric-varying system $\dot{x} = A(\delta)x$ with $\delta \in \mathcal{D}$ is exponentially stable if $\exists X \in \mathbb{R}^{6 \times 6}, X > 0$

$$A^\top(\delta)X + XA(\delta) < 0 \quad \forall \delta \in \mathcal{D}_l. \quad (27)$$

The origin is an exponentially stable equilibrium point for the nonlinear system (20) if it is an exponentially stable equilibrium point for the linear system $\dot{x} = Ax$ [27]. Thus, exponential stability for the nonlinear dynamic is also ensured in a local sense.

The stability condition derived in (27) implies an arbitrary time-varying parameter δ . If the rate of variation of δ is bounded, the aforementioned stability test is conservative. In our system, δ corresponds to the angular velocity of an object, and its rate of change can, in most cases, be considered to be bounded.

Similarly, we define $\hat{\delta} \triangleq [\hat{\delta}_1 \ \hat{\delta}_2 \ \hat{\delta}_3]^\top \in \mathcal{D}' = \text{co}(\hat{\delta}^1, \hat{\delta}^2, \dots, \hat{\delta}^8)$, where $\hat{\delta}^j$ denotes the vertices of a cube centered at zero (i.e., $\hat{\delta}^j \in \{\pm\hat{\delta}_{\max}, \pm\hat{\delta}_{\max}, \pm\hat{\delta}_{\max}\}$). We consider $\hat{\delta}$ to be bounded, i.e., $|\hat{\delta}_i| \leq \hat{\delta}_{\max}$, and we define the set of vertices $\mathcal{D}'_l = \{\hat{\delta}^1, \hat{\delta}^2, \dots, \hat{\delta}^8\}$. The autonomous part of (24), $\dot{x} = Ax$, is exponentially stable in the large, if there exist X_0, X_1, \dots, X_p with $A_\nu^\top X_\nu + X_\nu A_\nu \geq 0$, $\nu = 1, 2, \dots, m$ [33], such that

$$\sum_{k=0}^m X_k \delta_k > 0 \quad (28)$$

and

$$\sum_{k=1}^m X_k \hat{\delta}_k + \sum_{\nu=0}^m \sum_{\mu=0}^m \delta_\nu \delta_\mu (A_\nu^\top X_\mu + X_\mu A_\nu) < 0 \quad (29)$$

$\forall \delta \in \mathcal{D}_l$ and $\forall \hat{\delta} \in \mathcal{D}'_l$ and $\delta_0 = 1$. In this case, $m = 3$ (25).

The set of LMIs described in (27)–(29) can be solved using any semidefinite programming suite (e.g., SeDuMi [35]) in standard computational platforms, such as Python (e.g., cvxpy [36]), MATLAB (e.g., Yalmip [37]), and so on.

In summary, in the linear case (11), which corresponds to particular configurations of the accelerometers, the stability of the proposed system is easily ensured (see Section III-B,

² > 0 denote a positive-definite matrix.

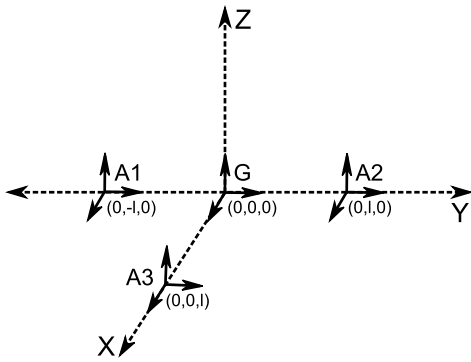


Fig. 3. IMU configuration composed of nine single-axis accelerometers (grouped in three three-axis ones) and a single three-axis gyroscope.

and only small attention is required on the design of the feedback’s filter. However, for an arbitrary configurations of the accelerometers, we notice that there is a nonlinear feedback term (6), which introduces a time-varying block, as shown in (24). This implies that the stability of the system relies on the sensors’ configuration. On the one hand, there is more freedom for the sensor structure to be selected, but, on the other hand, one has to be careful to guarantee stability for the custom configuration.

IV. PERFORMANCE EVALUATION

In this section, the performance of the proposed architecture is evaluated using both simulations and experimental measurements. In addition, the restrictions imposed by the previously derived stability conditions to the sensors’ placement and the design of the feedback filter are highlighted.

A. Noise Performance

To evaluate the noise characteristics of the proposed architecture, we consider the system configuration of Fig. 3. The feedback’s gain is set to $g = 10$, while the cutoff frequency of the low-pass filter is set to $p = 6\pi$ rads/s (3 Hz).

Using MATLAB’s Simulink, we simulated the described configuration assuming white noise sequences for both the accelerometers’ and the gyroscope’s inputs. The power spectral density (PSD) of the output noise for all accelerometers is set to be equal to $S_A = -50$ dB/Hz, while the PSD of all gyroscope’s axes is $S_G = -65$ dB/Hz.

We use the noise model introduced in [17] to derive the PSD of the estimated angular velocity noise, which is shown in Fig. 4, for two different values of the parameter l in Fig. 3. In Fig. 4, it is shown that greater distance between the accelerometers (l) leads to significantly lower angular velocity noise in the higher frequencies where the output is dominated by the accelerometers’ measurements.

B. Experimental Results

The performance of the proposed system in real-world conditions is tested using the experimental setup, shown in Fig. 5. The experimental setup is composed of four low-cost inertial sensors (LSM9DS1 system-in-package (SiP) by STMicroelectronics) mounted on a laser-cut steel frame. In Table I, the

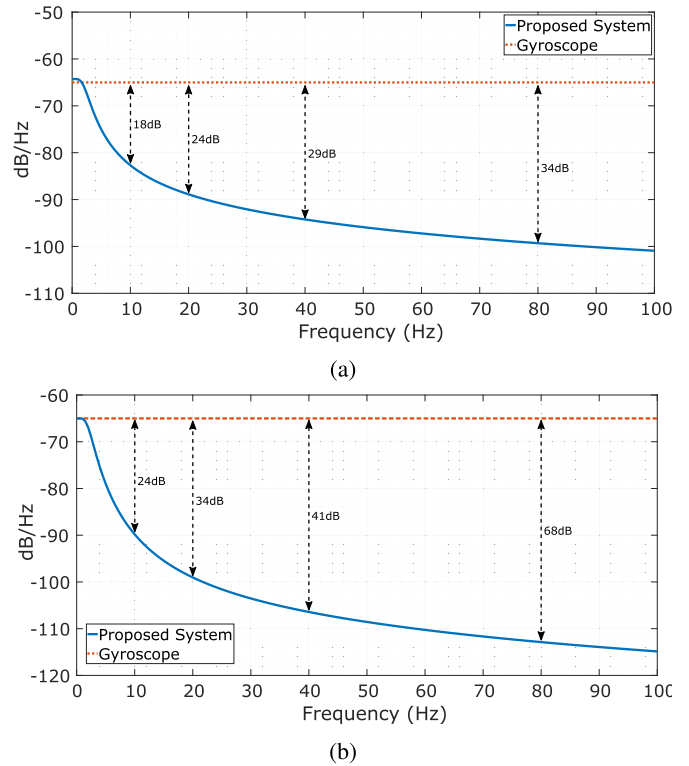


Fig. 4. PSD of the proposed system’s output noise (X-axis) compared with the PSD of the gyroscope’s output noise (X-axis) for (a) $l = 1$ m and (b) $l = 4$ m.

TABLE I
PERFORMANCE CHARACTERISTICS OF THE ACCELEROMETER (A) AND THE GYROSCOPE (G) EMBEDDED IN THE LSM9DS1 SiP

Specification	Value
Measurement Range (A)	± 16 g
Measurement Range (G)	± 2000 deg/s
Sampling Rate (A)	238 Hz
Sampling Rate (G)	238 Hz
Resolution (A, G)	16 Bits

most important performance characteristics of the LSM9DS1 SiP are presented.

The effect of sensors’ bias and noise is first examined by capturing the output of the accelerometers and the gyroscope of the designed IMU, while the IMU is still. In Fig. 6, the output angular velocity of the standard gyroscope-free, open-loop approach, without using the gyroscope at the origin, is compared with the output of the proposed closed-loop system. The output of the proposed closed-loop architecture exhibits a small, constant over time bias in contrast to the output of the open-loop system, which rises over time.

The noise performance of the proposed architecture is also evaluated using the experimental setup of Fig. 5. More specifically, accelerometers’ and gyroscope’s measurements were captured, while the platform was still to derive the PSD of the estimated angular velocity noise, which is shown in Fig. 7, and compared with the PSD of the gyroscope’s output noise. As shown in Fig. 7, the noise PSD of the estimated

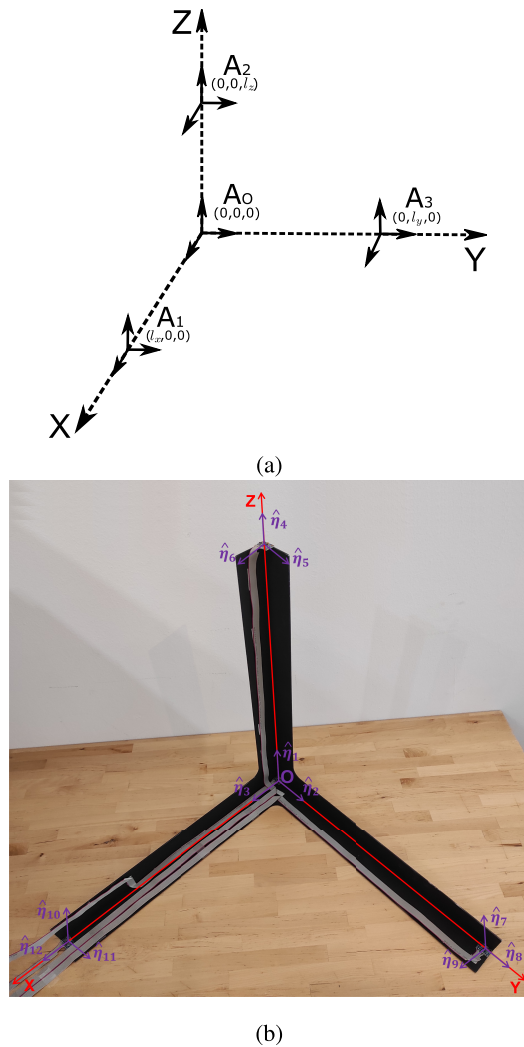


Fig. 5. Experimental setup composed of 12 (single-axis) accelerometers—grouped in four three-axis ones with $l_x = l_y = l_z = 0.5$ m.

angular velocity is significantly lower compared with the one of the gyroscope's outputs, confirming the simulation results.

Finally, the dynamic response of the system is evaluated. To this end, we rotated the setup of Fig. 5 by hand and captured the accelerometers' and gyroscope's measurements. Using them, we estimated the angular velocity of the sensors' platform and compared it with the gyroscope's measurements, as shown in Fig. 8. The output of the proposed system successfully tracks the gyroscope's measurements in low frequencies, while, zooming into the data, the noise suppression in the higher frequencies is revealed.

C. System Design and Stability Considerations

In Section IV-A, we demonstrated that the angular velocity noise of the proposed IMU becomes lower when the accelerometers are spread over a wider distance. In this section, we will examine the effect of the feedback filter's design on the output noise, and furthermore, we will demonstrate how improper design of the filter may lead to an unstable system.

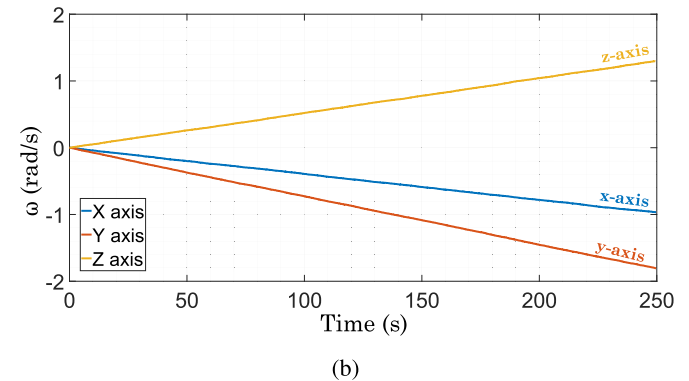
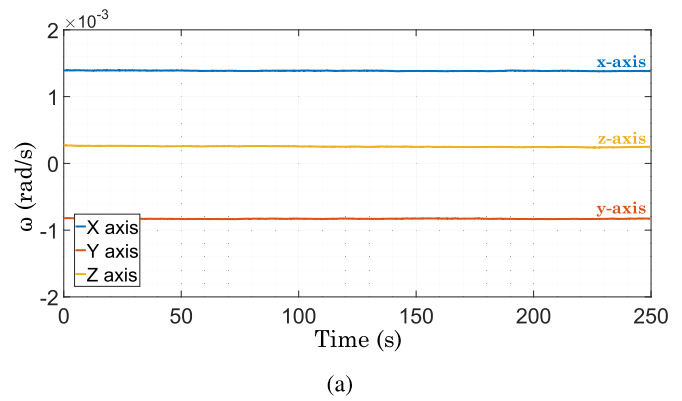


Fig. 6. (a) Output angular velocity of the proposed system compared with (b) output angular velocity of the standard gyroscope-free, open-loop system under the effects of measurement noise and bias.

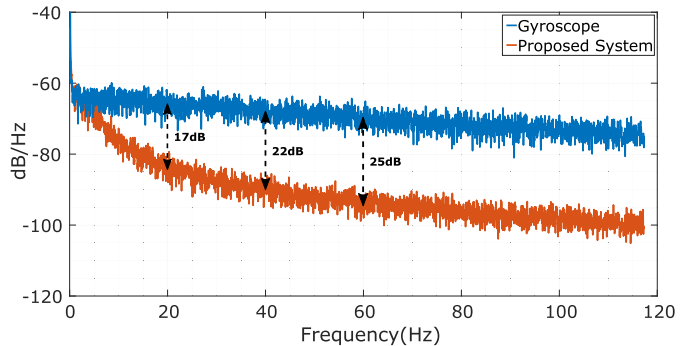


Fig. 7. PSD of the proposed system's output noise (X-axis) compared with the PSD of the gyroscope's output noise using the experimental setup of Fig. 5.

We assume the configuration of Fig. 3, and we consider the sensors' distance to be equal to $l = 2$ m. The power of the system's angular velocity noise in a 100-Hz bandwidth is presented in Tables II–V for different values of the maximum angular velocity (ω_{\max}) and the feedback filter's pole ($f_p = p/2\pi$) and gain (g) parameters. The configurations for which the stability cannot be guaranteed using (27) are denoted with “X” in Tables II–V.

In Table II, for $\omega_{\max} = 1$ rad/s, the system is stable for every pair (f_p, g), and the filter's design only affects the output noise power, which varies from -61.9 up to -53.3 dB. Note the lowest noise power of -61.9 dB is more than 15 dB lower than the output noise of the gyroscope in the same bandwidth. While the value of ω_{\max} gets higher, the stability of the system

TABLE II

ANGULAR VELOCITY NOISE WITHIN [0, 100] Hz FOR $\omega_{MAX} = 1$ rad/s AND DIFFERENT VALUES OF f_p AND g

	$g = 5$	$g = 10$	$g = 20$	$g = 50$
$f_p = 0.2\text{Hz}$	-58.0dB	-57.4dB	-56.1dB	-53.3dB
$f_p = 1\text{Hz}$	-60.9dB	-59.8dB	-57.6dB	-54.1dB
$f_p = 2\text{Hz}$	-61.4dB	-60.2dB	-57.9dB	-54.2dB
$f_p = 5\text{Hz}$	-61.9dB	-60.5dB	-58.0dB	-54.3dB
Gyroscope	-45.3dB			

TABLE III

ANGULAR VELOCITY NOISE WITHIN [0, 100] Hz FOR $\omega_{MAX} = 5$ rad/s AND DIFFERENT VALUES OF f_p AND g

	$g = 5$	$g = 10$	$g = 20$	$g = 50$
$f_p = 0.2\text{Hz}$	X	X	X	X
$f_p = 1\text{Hz}$	-60.9dB	-59.8dB	-57.6dB	-54.1dB
$f_p = 2\text{Hz}$	-61.4dB	-60.2dB	-57.9dB	-54.2dB
$f_p = 5\text{Hz}$	-61.9dB	-60.5dB	-58.0dB	-54.3dB
Gyroscope	-45.3dB			

TABLE IV

ANGULAR VELOCITY NOISE WITHIN [0, 100] Hz FOR $\omega_{MAX} = 7$ rad/s AND DIFFERENT VALUES OF f_p AND g

	$g = 5$	$g = 10$	$g = 20$	$g = 50$
$f_p = 0.2\text{Hz}$	X	X	X	X
$f_p = 1\text{Hz}$	X	X	X	-54.1dB
$f_p = 2\text{Hz}$	X	-60.2dB	-57.9dB	-54.2dB
$f_p = 5\text{Hz}$	X	-60.5dB	-58.0dB	-54.3dB
Gyroscope	-45.3dB			

TABLE V

ANGULAR VELOCITY NOISE WITHIN [0, 100] Hz FOR $\omega_{MAX} = 10$ rad/s AND DIFFERENT VALUES OF f_p AND g

	$g = 5$	$g = 10$	$g = 20$	$g = 50$
$f_p = 0.2\text{Hz}$	X	X	X	X
$f_p = 1\text{Hz}$	X	X	X	X
$f_p = 2\text{Hz}$	X	X	-57.9dB	-54.2dB
$f_p = 5\text{Hz}$	X	-60.5dB	-58.0dB	-54.3dB
Gyroscope	-45.3dB			

depends more on the design of the feedback’s filter. However, even in the case of $\omega_{max} = 10$ rad/s (Table V), proper design of the feedback filter leads to a stable configuration with only 1.4-dB more noise power (−60.5 dB), which is still about 15 dB lower than the output noise of the gyroscope in the same bandwidth.

As expected from classical control, picking a high gain “facilitates” the stability condition [27] but deteriorates noise performance, as shown in Tables II–V. In this article, two approaches for matching (g, p) parameters are suggested; one computation-based and one tuning-based. For the former, one has to create a grid of (g, p) values, as the one illustrated in Tables II–V, using simulations, which are cheap in the sense of time and processing. This procedure can be further automatized and optimized using an optimization algorithm, such as particle swarm optimization (PSO) [38], to find the best matching. For a less computational approach, one can select a high gain value and tune the p value manually to improve the noise performance. From this point onward, p

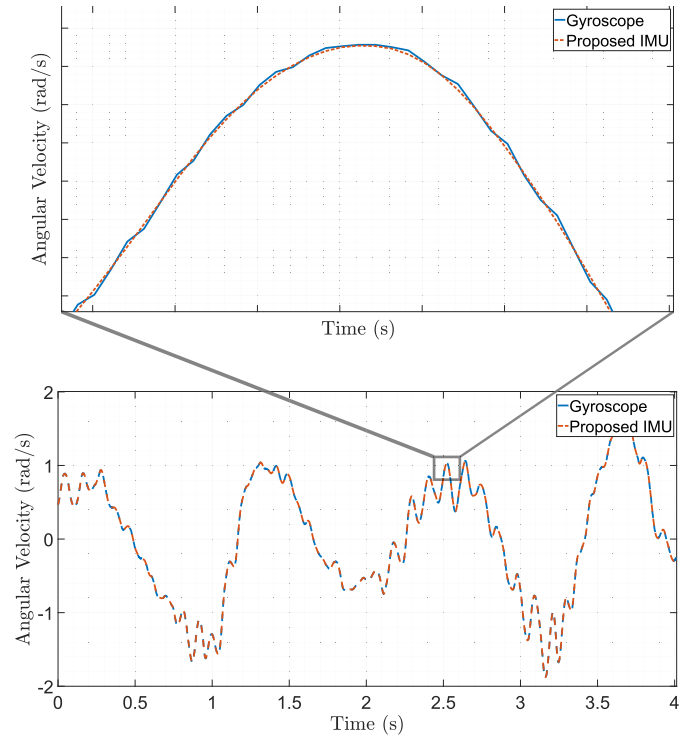


Fig. 8. Output angular velocity of the proposed system (x -axis) compared with the output angular velocity of the gyroscope (x -axis), while the platform is rotated by hand.

is fixed. Afterward, the user decreases the gain up to the point that stability is not guaranteed. The last value of gain g ensuring stability suits. This method is easily applicable to all the tables presented.

V. CONCLUSION

An IMU architecture using several accelerometers and a single three-axis gyroscope was introduced. The proposed architecture combines the low-noise characteristic of GF-IMUs and ensures the systems stability and immunity to the accelerometers’ bias by using the gyroscope in a closed-loop configuration. The extensive theoretical analysis as well as simulation and experimental results indicated that the proposed system is capable of providing up to 15 dB less angular velocity noise in its output compared with a gyroscope of the same grade, while its stability can be guaranteed when it is carefully designed. The GF-IMUs were extensively studied over the past years, but their inherent disadvantage to compensate for the accelerometers’ bias made the inappropriate for real-world applications despite their very good noise performance. The proposed architecture provides a solution to this problem and enables the development of low-noise, high-performance IMUs.

REFERENCES

- [1] P. D. Groves, *Principles of GNSS, Inertial, and Multisensor Integrated Navigation Systems*. Norwood, MA, USA: Artech House, 2013.
- [2] K. Papafotis and P. P. Sotiriadis, “MAG.I.C.AL.—A unified methodology for magnetic and inertial sensors calibration and alignment.” *IEEE Sensors J.*, vol. 19, no. 18, pp. 8241–8251, Sep. 2019.

- [3] J.-O. Nilsson, I. Skog, and P. Händel, "Aligning the forces—Eliminating the misalignments in IMU arrays," *IEEE Trans. Instrum. Meas.*, vol. 63, no. 10, pp. 2498–2500, Oct. 2014.
- [4] D. Tedaldi, A. Pretto, and E. Menegatti, "A robust and easy to implement method for IMU calibration without external equipments," in *Proc. IEEE Int. Conf. Robot. Autom. (ICRA)*, May 2014, pp. 3042–3049.
- [5] O. Särkkä, T. Nieminen, S. Suuriniemi, and L. Kettunen, "A multi-position calibration method for consumer-grade accelerometers, gyroscopes, and magnetometers to field conditions," *IEEE Sensors J.*, vol. 17, no. 11, pp. 3470–3481, Jul. 2017.
- [6] J. Lee, D. Hanley, and T. Bretl, "Extrinsic calibration of multiple inertial sensors from arbitrary trajectories," *IEEE Robot. Autom. Lett.*, vol. 7, no. 2, pp. 2055–2062, Apr. 2022.
- [7] X. Li and Z. Li, "Vector-aided in-field calibration method for low-end MEMS gyros in attitude and heading reference systems," *IEEE Trans. Instrum. Meas.*, vol. 63, no. 11, pp. 2675–2681, Nov. 2014.
- [8] J. Rehder, J. Nikolic, T. Schneider, T. Hinzmänn, and R. Siegwart, "Extending kalibr: Calibrating the extrinsics of multiple IMUs and of individual axes," in *Proc. IEEE Int. Conf. Robot. Autom. (ICRA)*, May 2016, pp. 4304–4311.
- [9] E. Dorveaux, D. Vissière, A. Martin, and N. Petit, "Iterative calibration method for inertial and magnetic sensors," in *Proc. 48th IEEE Conf. Decis. Control (CDC) Held Jointly 2009 28th Chin. Control Conf.*, Dec. 2009, pp. 8296–8303.
- [10] T. Xu, X. Xu, D. Xu, Z. Zou, and H. Zhao, "Low-cost and efficient thermal calibration scheme for MEMS triaxial accelerometer," *IEEE Trans. Instrum. Meas.*, vol. 70, pp. 1–9, 2021.
- [11] A. V. Kozlov, I. E. Tarygin, A. A. Golovan, I. K. Shaymardanov, and A. A. Dzuev, "Calibration of an inertial measurement unit at changing temperature with simultaneous estimation of temperature variation coefficients: A case study on BINS-RT," in *Proc. 24th Saint Petersburg Int. Conf. Integr. Navigat. Syst. (ICINS)*, May 2017, pp. 1–3.
- [12] P. Groves, G. Pulford, C. Littlefield, D. Nash, and C. Mather, "Inertial navigation versus pedestrian dead reckoning: Optimizing the integration," in *Proc. 20th Int. Tech. Meeting Satell. Division Inst. Navigat.*, vol. 2, Sep. 2007, pp. 2043–2055.
- [13] J. Bird and D. Arden, "Indoor navigation with foot-mounted strapdown inertial navigation and magnetic sensors [emerging opportunities for localization and tracking]," *IEEE Wireless Commun.*, vol. 18, no. 2, pp. 28–35, Apr. 2011.
- [14] A. Nouredin, T. B. Karamat, and J. Georgy, *Fundamentals of Inertial Navigation, Satellite-Based Positioning and Their Integration*. Berlin, Germany: Springer-Verlag, 2013.
- [15] K. Papafotis and P. P. Sotiriadis, "Exploring the importance of sensors' calibration in inertial navigation systems," in *Proc. IEEE Int. Symp. Circuits Syst. (ISCAS)*, Oct. 2020, pp. 1–4.
- [16] *Inertial Sensors*. Accessed: Aug. 25, 2022. [Online]. Available: <https://www.vectornav.com/resources/inertial-navigation-primer/theory-of-operation/theory-inertial>
- [17] K. Papafotis, D. Nikitas, and P. P. Sotiriadis, "Improving gyroscope's noise performance using multiple accelerometers in a closed-loop configuration," *IEEE Sensors J.*, vol. 22, no. 22, pp. 22062–22068, Nov. 2022.
- [18] D. Nikitas, K. Papafotis, and P. P. Sotiriadis, "Improving gyroscope's noise performance by embedding it in a closed-loop involving multiple accelerometers," in *Proc. 11th Int. Conf. Modern Circuits Syst. Technol. (MOCAS)*, Jun. 2022, pp. 1–4.
- [19] A. J. Padgaonkar, K. W. Krieger, and A. I. King, "Measurement of angular acceleration of a rigid body using linear accelerometers," *J. Appl. Mech.*, vol. 42, no. 3, pp. 552–556, Sep. 1975, doi: 10.1115/1.3423640.
- [20] J.-H. Chen, S.-C. Lee, and D. B. DeBra, "Gyroscope free strapdown inertial measurement unit by six linear accelerometers," *J. Guid., Control, Dyn.*, vol. 17, no. 2, pp. 286–290, 1994, doi: 10.2514/3.21195.
- [21] F. Qin, J. Xu, and J. Sai, "A new scheme of gyroscope free inertial navigation system using 9 accelerometers," in *Proc. Int. Workshop Intell. Syst. Appl.*, May 2009, pp. 1–4.
- [22] J. Genin, J. Hong, and W. Xu, "Accelerometer placement for angular velocity determination," *J. Dyn. Syst., Meas., Control*, vol. 119, no. 3, pp. 474–477, Sep. 1997, doi: 10.1115/1.2801281.
- [23] A. Li, F. Qin, and J. Xu, "Gyroscope free strapdown inertial navigation system using rotation modulation," in *Proc. 2nd Int. Conf. Intell. Comput. Technol. Automat.*, vol. 3, Oct. 2009, pp. 611–614.
- [24] F.-J. Qin, J.-N. Xu, and A. Li, "A novel attitude algorithm for 12 accelerometer based g-fins using Hermite interpolation," in *Proc. Int. Conf. Measuring Technol. Mechatronics Automat.*, vol. 1, Mar. 2010, pp. 214–217.
- [25] E. Edwan, S. Knedlik, and O. Loffeld, "Constrained angular motion estimation in a gyro-free IMU," *IEEE Trans. Aerosp. Electron. Syst.*, vol. 47, no. 1, pp. 596–610, Jan. 2011.
- [26] G. Strang, *Linear Algebra and Its Applications*. Boston, MA, USA: Cengage Learning, 2007.
- [27] H. Khalil, *Nonlinear Systems*. London, U.K.: Pearson, 2001.
- [28] D. J. Leith and W. E. Leithead, "Survey of gain-scheduling analysis and design," *Int. J. Control*, vol. 73, no. 11, pp. 1001–1025, 2000.
- [29] P. S. G. Cisneros, S. Voss, and H. Werner, "Efficient nonlinear model predictive control via quasi-LPV representation," in *Proc. IEEE 55th Conf. Decis. Control (CDC)*, Dec. 2016, pp. 3216–3221.
- [30] D. Rotondo, F. Nejjari, and V. Puig, "Quasi-LPV modeling, identification and control of a twin rotor MIMO system," *Control Eng. Pract.*, vol. 21, no. 6, pp. 829–846, Jun. 2013. [Online]. Available: <https://www.sciencedirect.com/science/article/pii/S0967066113000142>
- [31] C. Briat, *Linear Parameter-Varying and Time-Delay Systems. Analysis, Observation, Filtering and Control*. Jan. 2015.
- [32] R. Toth, *Modeling and Identification of Linear Parameter-Varying Systems*. vol. 403, Oct. 2010.
- [33] J. Mohammadpour Velni and C. Scherer, *Control of Linear Parameter Varying Systems With Applications*. Jan. 2012.
- [34] S. Boyd and L. Vandenberghe, *Convex Optimization*. Cambridge, U.K.: Cambridge Univ. Press, 2013.
- [35] J. F. Sturm, "Using SeDuMi 1.02, a MATLAB toolbox for optimization over symmetric cones," *Optim. Methods Softw.*, vol. 11, nos. 1–4, pp. 625–653, 1999.
- [36] S. Diamond and S. Boyd, "CVXPY: A Python-embedded modeling language for convex optimization," *J. Mach. Learn. Res.*, vol. 17, no. 83, pp. 1–5, Apr. 2016.
- [37] J. Lofberg, "YALMIP: A toolbox for modeling and optimization in MATLAB," in *Proc. IEEE Int. Conf. Robot. Autom.*, Taiwan, Sep. 2004, pp. 284–289.
- [38] J. Kennedy and R. Eberhart, "Particle swarm optimization," in *Proc. Int. Conf. Neural Netw. (ICNN)*, vol. 4, Nov./Dec. 1995, pp. 1942–1948.



Konstantinos Papafotis (Member, IEEE) received the Diploma degree in electrical and computer engineering from the National Technical University of Athens, Athens, Greece, in 2015, under the supervision of Prof. Paul P. Sotiriadis.

His Ph.D. thesis is about calibration methods and applications of inertial and magnetic field sensors in the field of navigation. He has authored several conference papers and journal articles. His main research interests include inertial navigation, embedded systems, and wireless sensors' systems.

Dr. Papafotis has received the Best Paper Award in the IEEE International Conference on Modern Circuits and Systems Technologies in 2019. He is a regular reviewer for many IEEE publications.



Dimitris Nikitas (Graduate Student Member, IEEE) received the Diploma degree in electrical and computer engineering from the National Technical University of Athens, Athens, Greece, in 2021, under the supervision of Prof. Paul P. Sotiriadis. He is currently pursuing the M.Sc. degree in the field of systems and control from the Eindhoven University of Technology, Eindhoven, the Netherlands.

He has authored several conference and journal articles. His main research interests include control theory, robotics, and inertial navigation.

Prof. Nikitas was a Reviewer of the IEEE SENSORS JOURNAL. He is a regular reviewer for many IEEE publications.

Costas Oustoglou received the Diploma degree in electrical and computer engineering from the National Technical University of Athens, Athens, Greece, in 2017. He is currently pursuing the Ph.D. degree with the National Technical University of Athens, under the supervision of Prof. Paul P. Sotiriadis.

His main research interests include radiometry systems and applications, and design and development of embedded and mixed signal systems.

Mr. Oustoglou is a regular reviewer for many IEEE publications.



Paul P. Sotiriadis (Fellow, IEEE) received the Diploma degree in electrical and computer engineering from the National Technical University of Athens (NTUA), Athens, Greece, in 1994, the M.S. degree in electrical engineering from Stanford University, CA, USA, in 1996, and the Ph.D. degree in electrical engineering and computer science from the Massachusetts Institute of Technology, MA, USA, in 2002.

In 2002, he joined the faculty of the Johns Hopkins University Electrical and Computer Engineering Department and he joined the faculty of the Electrical and Computer Engineering Department of the NTUA, in 2012. He is a Professor of Electrical

and Computer Engineering of the NTUA, the Director of the Electronics Laboratory at the NTUA. He has authored and coauthored more than 200 research publications, most of them in IEEE journals and conferences, holds one patent, and has contributed several chapters to technical books. His research interests include the design, optimization, and mathematical modeling of analog, mixed-signal and RF integrated and discrete circuits, sensor and instrumentation architectures with emphasis in biomedical instrumentation, advanced RF frequency synthesis, integrated analog and mixed signal implementations of Machine Learning algorithms and application of Artificial Intelligence in the design of electronic circuits.

Dr. Sotiriadis is a Governing Board Member of the Hellenic (National) Space Center of Greece. He has been a member of technical committees of many conferences. He has received several awards, including the prestigious Guillemin-Cauer Award from the IEEE Circuits and Systems Society in 2012, the Best Paper Award in the IEEE International Symposium on Circuits and Systems in 2007, the Best Paper Award in the IEEE International Frequency Control Symposium in 2012, the Best Paper Award in the IEEE International Conferences on Modern Circuits and Systems Technology in 2019, the Best Paper Award in the IEEE International Conferences on Microelectronics (ICM) in 2020, the Best Paper Award in the IEEE International Conferences on Microelectronics (ICM) in 2021, the Best Paper Award in the IEEE Symposium on Integrated Circuits and Systems Design (SBCCI) in 2021, and the IEEE Circuits and Systems Society (CASS) Outstanding Technical Committee Recognition in 2022. He is an Associate Editor of the IEEE Sensors Journal and has served as an Associate Editor of the IEEE TRANSACTION ON CIRCUITS AND SYSTEMS - I in 2016 to 2020 and the IEEE TRANSACTION ON CIRCUITS AND SYSTEMS - II in 2005 to 2010, and has been a member of technical committees of many conferences. He regularly reviews for many IEEE TRANSACTIONS AND CONFERENCES AND SERVES ON PROPOSAL REVIEW PANELS.